

# Characterization of a Murine Model of Oxazolone-Induced Orbital Inflammation

Dhanesh Amarnani<sup>1,\*</sup>, Angie V. Sanchez<sup>1,\*</sup>, Lindsay L. Wong<sup>1</sup>, Brandon V. Duffy<sup>2</sup>, Leslie Ramos<sup>2</sup>, Suzanne K. Freitag<sup>3</sup>, Diane R. Bielenberg<sup>4</sup>, Leo A. Kim<sup>1,5,‡</sup>, and Nahyoung Grace Lee<sup>3,‡</sup>

<sup>1</sup> Schepens Eye Research Institute/Massachusetts Eye and Ear, Department of Ophthalmology, Harvard Medical School, Boston, MA, USA

<sup>2</sup> Harvard College, Cambridge, MA, USA

<sup>3</sup> Ophthalmic Plastic Surgery, Massachusetts Eye and Ear, Department of Ophthalmology, Harvard Medical School, Boston, MA, USA

<sup>4</sup> Vascular Biology Program, Boston Children's Hospital, Department of Surgery, Harvard Medical School, Boston, MA, USA

<sup>5</sup> Retina Service, Massachusetts Eye and Ear Infirmary, Department of Ophthalmology, Harvard Medical School, Boston, MA, USA

**Correspondence:** Nahyoung Grace Lee, 243 Charles St. 10th floor Eye Plastics, Boston, MA 02114, USA. e-mail: [grace\\_lee@meei.harvard.edu](mailto:grace_lee@meei.harvard.edu)  
Leo A. Kim, 20 Staniford St., Boston, MA 02114, USA. e-mail: [leo\\_kim@meei.harvard.edu](mailto:leo_kim@meei.harvard.edu)

**Received:** July 9, 2019

**Accepted:** May 4, 2020

**Published:** July 16, 2020

**Keywords:** orbital inflammation; murine model; Graves' disease; thyroid eye disease

**Citation:** Amarnani D, Sanchez AV, Wong LL, Duffy BV, Ramos L, Freitag SK, Bielenberg DR, Kim LA, Lee NG. Characterization of a murine model of oxazolone-induced orbital inflammation. *Trans Vis Sci Tech*. 2020;9(8):26, <https://doi.org/10.1167/tvst.9.8.26>

**Purpose:** Acute orbital inflammation can lead to irreversible vision loss in serious cases. Treatment thus far has been limited to systemic steroids or surgical decompression of the orbit. An animal model that mimics the characteristic features of acute orbital inflammation as found in thyroid eye disease can be used to explore novel treatment modalities.

**Methods:** We developed a murine model of orbital inflammation by injecting oxazolone into the mouse orbit. The mice underwent magnetic resonance imaging (MRI) and were euthanized at various time points for histologic examination. Immunofluorescence studies of specific inflammatory cells and cytokine arrays were performed.

**Results:** We found clinical and radiographic congruity between the murine model and human disease. After 72 hours, sensitized mice exhibited periorbital dermatitis and inflammation in the eyelids of the injected side. By one week, increased proptosis in the injected eye with significant eyelid edema was appreciated. By four weeks, inflammation and proptosis were decreased. At all three time points, the mice demonstrated exophthalmos and periorbital edema. Histopathologically, populations of inflammatory cells including T cells, macrophages, and neutrophils shared similarities with patient samples in thyroid eye disease. Proteomic changes in the levels of inflammatory and angiogenic markers correlated to the expected angiogenic, inflammatory, and fibrotic responses observed in patients with thyroid eye disease.

**Conclusions:** A murine model of orbital inflammation created using oxazolone recapitulates some of the clinical features of thyroid eye disease and potentially other nonspecific orbital inflammation, typified by inflammatory cell infiltration, orbital tissue expansion and remodeling, and subsequent fibrosis.

**Translational Relevance:** This animal model could serve as a viable platform with which to understand the underlying mechanisms of acute orbital inflammation and to investigate potential new, targeted treatments.

## Introduction

Orbital inflammation is a common clinical entity that has the potential to cause significant morbidity including permanent vision loss, diplopia, and periorbital disfigurement due to edema and subsequent fibro-

sis. Thyroid eye disease (TED) is the most common cause of orbital inflammation seen in adults,<sup>1</sup> with nonspecific orbital inflammation (NSOI) being the second-most common.<sup>2</sup> Elucidating the pathophysiology of orbital inflammation has challenged clinicians and scientists for decades, which explains why treatment options are still limited. Animal models of disease

conditions can facilitate the development of new treatment paradigms, yet there have been no reliable models of orbital inflammation thus far.

In the past two decades, there have been attempts to create a TED mouse model via the following three mechanisms: immunizing mice with human thyroid stimulating hormone receptor (TSHR)-transfected fibroblasts, infecting mice with an expression plasmid containing human TSHR cDNA, and injecting an adenoviral vector expressing human TSHR.<sup>3,4</sup> These attempts have been variably successful; however, the ocular features of TED were not consistently present. In 2011, Zhao and colleagues<sup>5</sup> were able to immunize mice with plasmids encoding TSHR A, which induced hyperthyroidism and orbital fibrosis on histopathology but failed to exhibit the clinical phenotype of TED. Similarly, Moshkelgosha and colleagues<sup>6</sup> demonstrated orbital congestion associated with TED by injecting plasmid-containing TSHR followed by electroporation of mouse thigh skeletal muscle. However, the histopathology of optic nerve infiltration of inflammatory cells in these models was not consistent with human TED. Therefore a consistent orbital phenotype of TED has not been reliably demonstrated with a systemic insult. The only direct model of idiopathic or nonspecific orbital inflammation in animals was created in 1987 by injecting 12-0-tetradecanoyl-phorbol-13-acetate (TPA) into the superior rectus muscle of New Zealand white rabbits.<sup>7</sup> This model produced acute inflammation (myositis) and edema within 48 hours, followed by fibrosis and muscle restriction by 12 weeks. Further studies on this model with potential treatment paradigms have not been attempted. Overall, these models have shown inconsistent results and clinical deviation from human orbital disease. Hence, our goal was to devise a comparable milieu in the mouse orbit to eventually serve as an experimental platform for the elucidation of the molecular mechanisms of orbital inflammatory diseases and the development of novel targeted therapies.

Oxazolone is a potent skin sensitizer that induces a type 4 hypersensitivity reaction. It has been used since 1968 to induce contact dermatitis<sup>8-11</sup> in mice, as well as create a murine model of ulcerative colitis.<sup>12</sup> Studies that induce this delayed-type of contact sensitivity in mice with oxazolone have shown that there is an initial spike in tumor necrosis factor (TNF) and interferon- $\gamma$  (IFN $\gamma$ ) followed by increased levels of interleukin-4 (IL-4) with long-term exposure.<sup>13,14</sup> Analogous to these aforementioned models, oxazolone was used in our study to incite inflammation in the mouse orbit as a new model of acute orbital inflammation. To examine how closely this model of orbital inflammation parallels human orbital inflammatory entities, we compared mouse orbits to human orbital adipose

specimens from patients with acute or chronic TED undergoing orbital decompression surgery. Due to the variegated nature of nonspecific orbital inflammation and lack of specific etiology, TED specimens were preferentially used for a more consistent comparison. In our human studies, we demonstrated an increase in blood vessel formation and lymphatic vessel formation in patients with acute TED compared to patients with chronic TED and in control specimens without TED.<sup>15</sup> Based on these results, we searched for the formation of new blood and lymphatic vessels via angiogenesis and lymphangiogenesis-related markers in our mouse model. In addition, we compared the presence or absence of specific inflammatory cells to assess the congruity between the human and murine environments and evaluated cytokine markers that are frequently involved in human orbital inflammatory conditions.

## Methods

### Animal Model

Eight-week-old female BALB/c mice (Jackson Laboratory, Bar Harbor, ME, USA) were housed in our animal research facility in accordance with the Institutional Animal Care and Use Committee guidelines and the Association for Research in Vision and Ophthalmology Animal Statement. The mice were sensitized by a topical application of 2% oxazolone (4-ethoxymethylene-2-phenyl-2-oxazolone-5-one; E0753, Sigma-Aldrich, St. Louis MO, USA) solution in olive oil/acetone (2:1 vol/vol) to the shaved abdomen. Five days after sensitization, the right orbit was challenged by a sub-Tenon's retrobulbar injection with 5 microliters of 2% oxazolone solution using a 30-gauge, 1/2-inch needle. Uninjected left eyes served as a control group for this study. Additional experimental controls including oxazolone-sensitized phosphate-buffered saline solution (PBS)-injected eyes; oxazolone-sensitized olive oil/acetone vehicle-injected eyes; and eyes from nonsensitized oxazolone-injected eyes were also analyzed to evaluate the presence of inflammatory cells, blood and lymphatic vessels in our model (Figs. S2-S5). Three mice per group were euthanized at three time points after oxazolone injection: 72 hours, one week, and four weeks, and one sensitized mouse at each time point also underwent magnetic resonance imaging (MRI) just before euthanasia. Tissue from orbital exenterations was fixed in 4% paraformaldehyde (PFA; 15714-5, Electron Microscopy Sciences) to perform histopathologic and immunohistochemical analysis.

## MRI

In vivo MRI was performed on mice using a 4.7 Tesla Bruker Pharmascan mouse MRI at 72 hours, one week, and four weeks after oxazolone injection. The dorsal tail vein was used for injection of the gadolinium contrast. Mice were anesthetized with inhaled isoflurane (1%–3% mixed with oxygen). They were then placed in the MRI holder, and a brain radiofrequency coil was used to obtain high-resolution imaging. Mouse heart rate, respiration rate, and temperature were monitored throughout the scan while T<sub>1</sub>- and T<sub>2</sub>-weighted axial and coronal images with and without gadolinium contrast were acquired.

## Histopathology

Mouse orbits were exenterated by performing a midline, sagittal craniotomy with a no. 10 blade to separate the right from the left orbit. Toothed forceps and scissors were used to gently extract the orbital contents from fragments of surrounding bone. Orbits were fixed in 4% PFA overnight at room temperature and then stored in Dulbecco's PBS (PBS, D5652-10X1L; Sigma-Aldrich) at 4°C and processed before paraffin embedding. Centering the specimen on the optic nerve, the orbital tissue was oriented for sagittal paraffin sections.

## Human Specimen Collection

The collection of orbital fat sample from patients with acute and chronic TED has been obtained as previously described under an IRB approved protocol.<sup>15</sup> Tissue was fixed in 4% PFA overnight, followed by three rinses using PBS. Specimens were stored in PBS at 4°C and processed for paraffin embedding. Serial sections were cut to perform staining.

## Immunofluorescence Staining

Sections were deparaffinized in 100% xylene, rehydrated using a series of graded ethanols, and rinsed with PBS. Heat-induced epitope retrieval was performed with citrate buffer pH6 (Vector Laboratories, Burlingame, CA, USA) and sections were incubated for 20 minutes, followed by 20 minutes of cool down. After washing with PBS, sections were blocked for one hour at room temperature (RT) using blocking buffer composed of 0.01% Triton X-100 (T8787-100ML; Sigma-Aldrich), 10% donkey serum (017-000-121, Jackson ImmunoResearch Laboratories) or goat serum (G9023-10ML, Sigma-Aldrich), and PBS. The primary antibodies, Ly6G (ab25377, 1:100; abcam), IBA1 (ab5076, 1:100; abcam), CD3 (ab5076,

1:100; abcam), CD20 (MA5-13141, 1:100; Thermo Fisher Scientific, Waltham, MA, USA), endomucin (ab106100, 1:100; abcam), podoplanin (103-PA40S, 1:50; Relia-Tech, Andover, MA, USA), and VEGFR3 (ab27278, 1:100; abcam) were incubated overnight at 4°C. The following day, sections were rinsed with PBS and incubated for two hours in secondary antibodies as follows: Alexa Fluor-594 donkey anti-goat (A11058, 1:300; Invitrogen, Carlsbad, CA, USA), Alexa Fluor-594 donkey anti-rabbit (A21207, 1:200; Invitrogen), Alexa Fluor-594 donkey anti-rat (A21207, 1:200; Invitrogen), Alexa Fluor-488 goat anti-mouse (A11001, 1:200; Invitrogen). Prolong Gold antifade mount with DAPI (P36935, Thermo Fisher Scientific) was used for nuclear staining and mounting.

## Cytokine Array Analysis

Mouse orbital fat tissues were collected 72 hours, one week, and four weeks after oxazolone injection, digested, and homogenized in PBS with 1X Protease Cocktail Inhibitor (Cell Signaling Technology, Danvers, MA, USA) and Triton X-100. Protein concentrations were quantified and 200ug of protein was processed on the Mouse Proteome Profiler Cytokine Array Kit (Catalog Number ARY028; R&D Systems, Minneapolis, MN, USA). The experimental setup included membranes for each sample; two PBS-injected controls and two oxazolone-injected experimental orbits were used for each time point. Dot blot analysis was performed via Image J by measuring integrated density. Background was accounted for by subtracting the integrated density of the dot's surrounding area. A variance analysis was conducted on each array (Fig. 5) to identify potential candidate proteins, as previously described.<sup>16</sup> Proteins of interest were considered differentially abundant in the tissue at a specific time point if the absolute value of the difference between the control and experimental conditions exceeded 1.5 times the variance (equation below), and the direction of the change was concordant between both mice.

$$Var = \sqrt{\frac{(Control_1 - Control_2)^2 + (Experimental_1 - Experimental_2)^2}{2}}$$

## Results

### Sub-Tenon's Oxazolone Injection Induces Orbital Inflammation

Nine mice were sensitized topically on the abdomen (Fig. 1A), challenged with a unilateral right-sided sub-Tenon's injection of 2% oxazolone on day 0

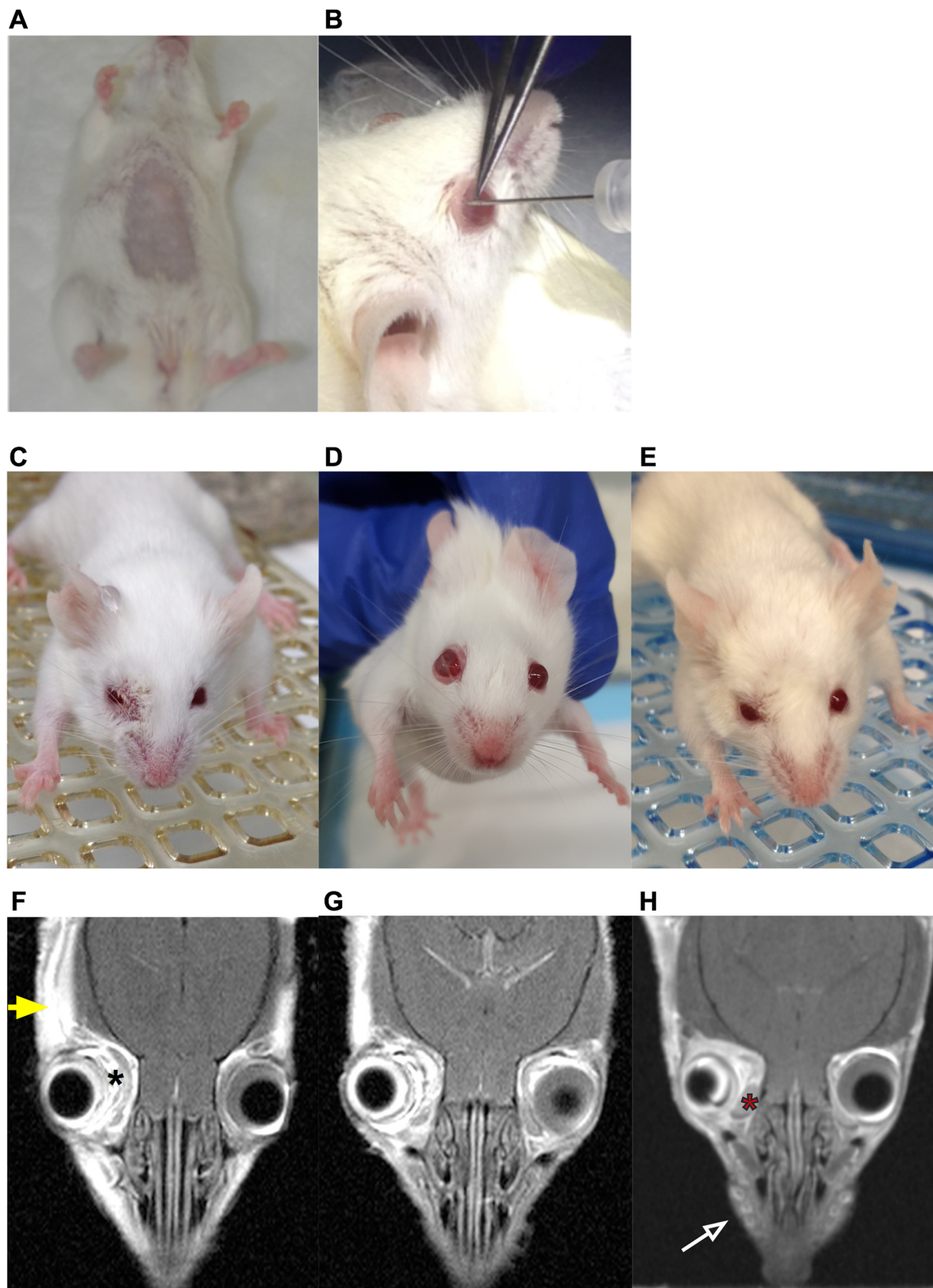


**Figure 1.** Phenotype of oxazolone-induced orbital inflammation (A) Oxazolone sensitization occurred with a topical application of 2% oxazolone on the shaved abdomen. (B) Five days later, oxazolone challenge performed with a 30-gauge needle as a sub-Tenon's injection (day 0). (C) 72 hours after injection of 2% oxazolone in the right orbit demonstrates inflammation and edema of the right face and periocular region with dermatitis. (D) Week 1 mouse exhibits exophthalmos of the right eye with erythema and edema of the eyelids with decreased facial swelling. (E) Week 4 mouse manifests improved exophthalmos with mild residual dermatitis. (F) Mouse T<sub>2</sub>-weighted MRI at 72 hours

→

← reveals dramatic hyperintensity along the right face toward the nose (yellow arrow) with significant retrobulbar edema and inflammation (black asterisk). (G) Week 1 MRI demonstrates improved facial inflammation but increased exophthalmos and persistent hyperintense retrobulbar tissue. (H) Week 4 MRI shows near complete improvement in the facial inflammation (white arrow) with some residual adnexal expansion of tissue yet decreased hyperintensity compared to week 1; (red asterisk marks Harderian gland).

(Fig. 1B), and then observed every hour for the first 24 hours. Three mice were euthanized at three different time points: 72 hours, one week, and four weeks after injection. After 72 hours, the sensitized mice exhibited periorbital dermatitis and inflammation in the upper and lower eyelids of the injected side as observed in Figure 1C. By one week, the clinical manifestation of proptosis in the right eye with eyelid edema was appreciated (Fig. 1D). By four weeks, the inflammation and proptosis were decreased, but still present (Fig. 1E). These clinical findings were contrasted to the opposite uninjected orbits of the mice, which did not demonstrate any phenotypic changes.

### MRI Reveals Inflammatory Orbitopathy in Oxazolone Treated Mice

Before euthanasia, mice underwent MRI 72 hours, one week, and four weeks after injection, which corroborated the findings of exophthalmos and periorbital edema. There was marked edema and inflammation in the preseptal and postseptal tissues including the right facial soft tissue, right extraocular muscles (EOM), and retrobulbar tissue at 72 hours (Fig. 1F). There was decreased hyperintensity and edema by week 1 (Fig. 1G), which was further decreased by week 4 (Fig. 1H). However, the injected right side continued to remain more inflamed in comparison to the left side.

### Histopathology Confirms Oxazolone-Induced Orbital Inflammation

Mice were euthanized at 72 hours, one week, and four weeks. Their orbits were exenterated and fixed at each of these time points. At 72 hours, there was infiltration of inflammatory cells within the eyelid and postseptal tissue (Figs. 2A, 2B). Further examination of the retrobulbar space revealed focal involvement of inflammatory cells in the striated EOMs and orbital adipose tissue. At one week, there was marked infiltration of inflammatory cells with mass effect diffusely in the orbital tissue with effacement of normal architecture. By four weeks, there were fewer inflammatory cells and signs of early fibrosis (Figs. 2A, 2B).

### Identification of Inflammatory Cells By Immunofluorescence Staining

Although hematoxylin and eosin revealed the presence of inflammatory cells, immunofluorescence staining was used to determine the specific cell types and more clearly delineate the similarities between human TED and the mouse model. All specimens were co-stained with DAPI, to identify the nuclei of the cells. Immunofluorescence staining demonstrated that acute TED is characterized by the presence of neutrophils (elastase), T cells (CD3), and a lack of B cells (CD20) and macrophages (IBA1), whereas the chronic phase of TED is positive for all four cell types (data not shown). Staining of neutrophils (Ly6g), T cells (CD3), B-cells (CD20), and macrophages (IBA1) was performed on the mouse model orbital tissue at 72 hours, 1 week, and 4 weeks. T cells, macrophages, and neutrophils were found at all 3 time points; however, there were no identifiable B cells within the mouse model at any time point (Fig. 3).

### Lymphatic and Blood Vessels were Identified in Oxazolone-Induced Orbital Inflammation

Immunofluorescence was used to determine whether lymphatic and blood vessels were present in the mouse model. Similar to human tissue, the normal mouse orbit is devoid of lymphatic vessels, which was corroborated in our nonsensitized mouse orbit specimens (Supplemental Fig. S1). However, lymphatic vessels (podoplanin+) are present surrounding the optic nerve at the early stage of the mouse model (72 hours and one week after injection), whereas they are not apparent at four weeks (Fig. 4 and Supplementary Fig. S5). Additionally, blood vessels (endomucin+) were observed within the retrobulbar adipose tissue at all 3 time points. These data showing increased presence of lymphatic vessels during the early phase of the disease, which diminishes over time, further suggesting a resemblance between the mouse model of orbital inflammation and human TED.<sup>15</sup>

### Expression of Cytokines in Oxazolone-Induced Orbital Inflammation

Most patients with TED have EOM and adipose tissue expansion due to cellular growth, migration,

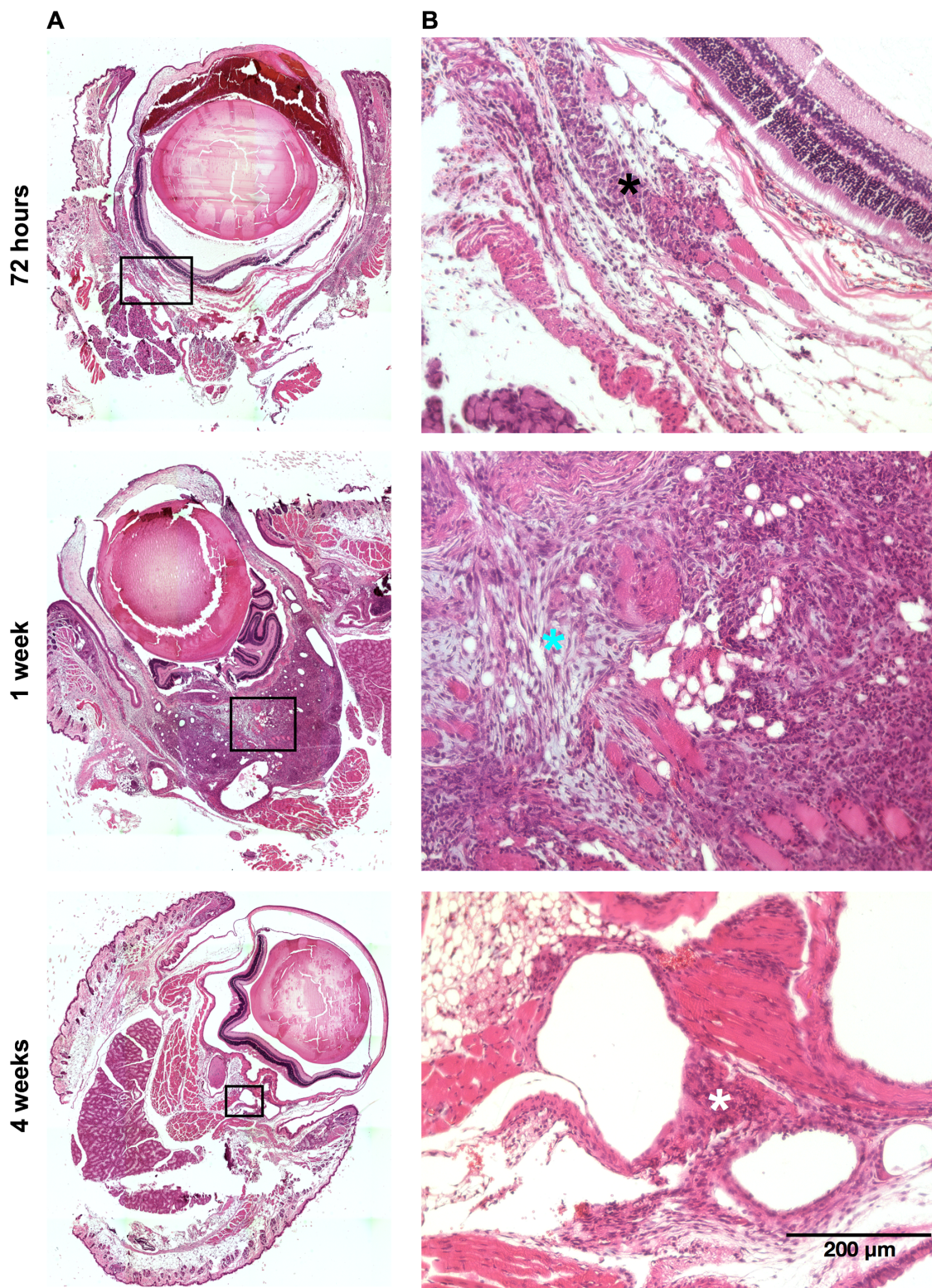


**Figure 2.** Histopathology of oxazolone-induced orbital inflammation. Hematoxylin-eosin stain of exenterated mouse orbit at 72 hours, one week, and four weeks after injection (column A: low power, column B: high power). At 72 hours, there are focal areas of inflammation within the exenterated specimen. Higher magnification of boxed area reveals retrobulbar, focal area of infiltrating inflammatory cells within the EOM and the adipose tissue. One week after injection, exenterated orbit demonstrates diffuse retrobulbar area of inflammation occupying nearly entire retrobulbar space and causing mass effect on globe. High magnification of boxed area reveals effacement of normal orbital tissue including EOM and adipose tissue as well as ingrowth of fibroblasts (blue asterisk). Four weeks after injection, exenterated orbit reveals diminished inflammatory infiltrate but with perineural areas of fibrosis and mild residual inflammation on higher power (white asterisk).

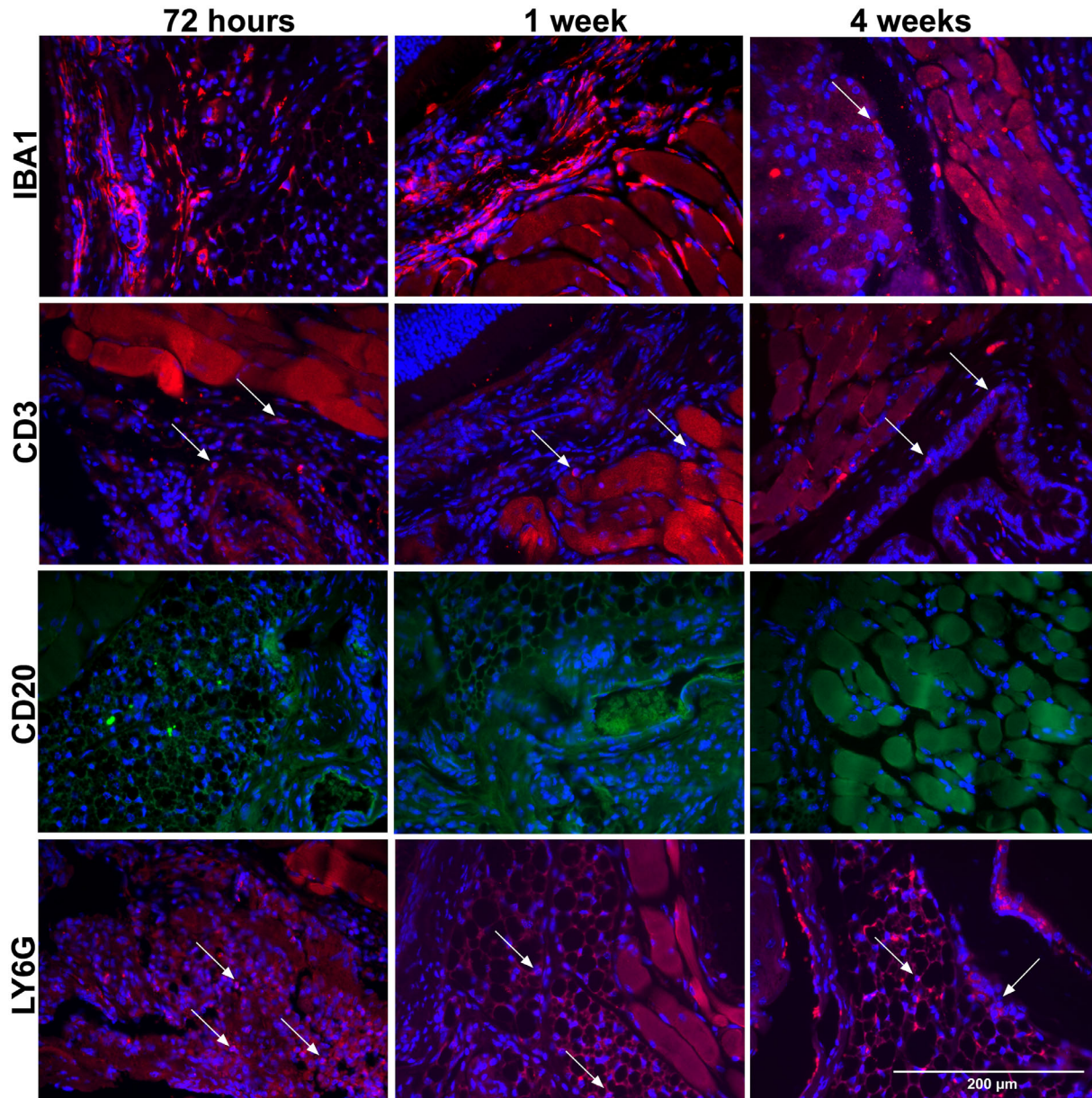


**Figure 3.** Immunofluorescence staining of orbital inflammatory cells in mouse model. Exenterated mouse orbital tissue centered around inflammatory cells seen on hematoxylin-eosin staining. IBA1 (red) was used to stain for macrophages and is positive at all three time points (72 hours, one week, and four weeks after injection) of the mouse model. Likewise, T cells stained via CD3 (red) were also identified in all the mouse tissue samples and all time points. Mouse orbit did not stain positive for B cells (CD20) at any time point (green). Ly6g (red) was used to identify mouse neutrophils. Neutrophil staining was positive at all three time points. DAPI was used to stain nuclei blue in all frames. Scale bars are 200  $\mu$ m.

extracellular matrix deposition, and inflammatory cell influx. We used an antibody mouse cytokine array with 111 different capture antibodies to determine whether candidate proteins involved in these pathways could be detected in the orbital tissue samples from our oxazolone-injected mice compared against uninjected mice.

Within 72 hours, our analyses showed a significant increase in acidic fibroblast growth factor (acidic

FGF). At the one-week time point, we identified a significant increase in pigment epithelium-derived factor (PEDF), a significant decrease in Cystatin C, and a significant increase in myeloperoxidase. At both the one-week and four-week time points, we identified a significant increase in endoglin. At four weeks we found decreased expression of Chitinase 3-like 1 (CHI3L1/YKL-40), increased expression of Reg3 $\gamma$ , increased expression of C-C motif chemokine ligand

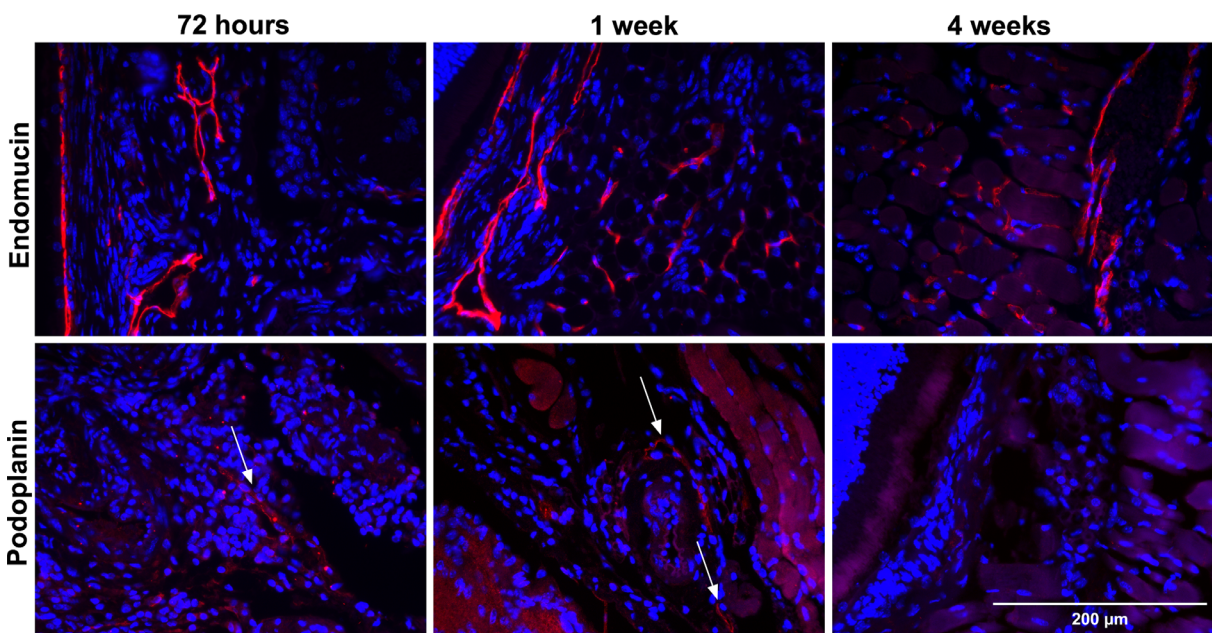


**Figure 4.** Lymphatic and blood vessel staining in mouse model. Blood vessels were stained using endomucin (red). All specimens, 72 hours, one week, and four weeks after injection, stained positive for endomucin surrounding the optic nerve. Podoplanin (red) was used to highlight lymphatic vessel formation. At 72 hours and one week after injection, lymphatic vessels were identified adjacent to the optic nerve (white arrows), while no lymphatic vessels were seen at four weeks after injection. DAPI was used to stain all nuclei blue. Scale bars are 200  $\mu\text{m}$ .

21 (CCL21), and decreased expression of insulin growth factor binding protein 2 (IGFBP-2) (Fig. 5, Table).

## Discussion

Orbital inflammatory diseases including TED are challenging conditions to manage given their poorly understood pathophysiology. Inflammation can affect a variety of orbital tissues including retrobulbar fat, extraocular muscles, optic nerve sheath, and surrounding adnexal structures such as the lacrimal gland. When orbital edema and tissue expansion reach a critical point in the confined bony orbit, diplopia, periorbital disfigurement and compressive optic neuropathy resulting in vision loss can ensue. Currently, the mainstays of treatment consist of systemic anti-inflammatory medications, such as systemic corticosteroids, orbital radiation, or decompression of the orbit by removing bone. None of these options are ideal, as they may have debilitating side effects, and surgery has risks including diplopia and vision loss. The lack of an animal model further limits our ability to develop experimental protocols to better understand the underlying mechanisms of orbital inflammatory disease.

One of the first mouse models of histopathologic TED was published in 1999 by Many and colleagues<sup>17,18</sup> by immunizing mice with TSHR-primed spleen cells. Although the findings of adipocyte proliferation, edema, and leukocytic infiltration were present microscopically, the mice failed to exhibit any phenotypic signs. Unfortunately, the model could not be reproduced by members of the same group.<sup>19</sup> Similarly, the models by Zhao and colleagues<sup>5</sup> and Moshkelgosha and colleagues<sup>6</sup> failed to consistently demonstrate the clinical orbital phenotype of Graves' disease. In contrast, all animals sensitized and treated with sub-Tenon's oxazolone exhibited some amount of orbital and periorbital inflammation. Our MRI findings in three mice with proptosis demonstrate significant edema and inflammation in the periorbital region, as well as in retrobulbar tissues at 72 hours persisting to one week.

Oxazolone has been used in animal models of inflammation from contact dermatitis to colitis. Because there are known associations between orbital inflammation and Crohn's colitis and ulcerative colitis,<sup>20</sup> this particular model has the potential to embody the same pathophysiology, but in a different location. Studies have shown that oxazolone mediates a Th2 response, much like chronic TED.<sup>9</sup> Moreover, Crohn's disease and Hashimoto's thyroiditis (one cause of TED) are also considered to be delayed-type

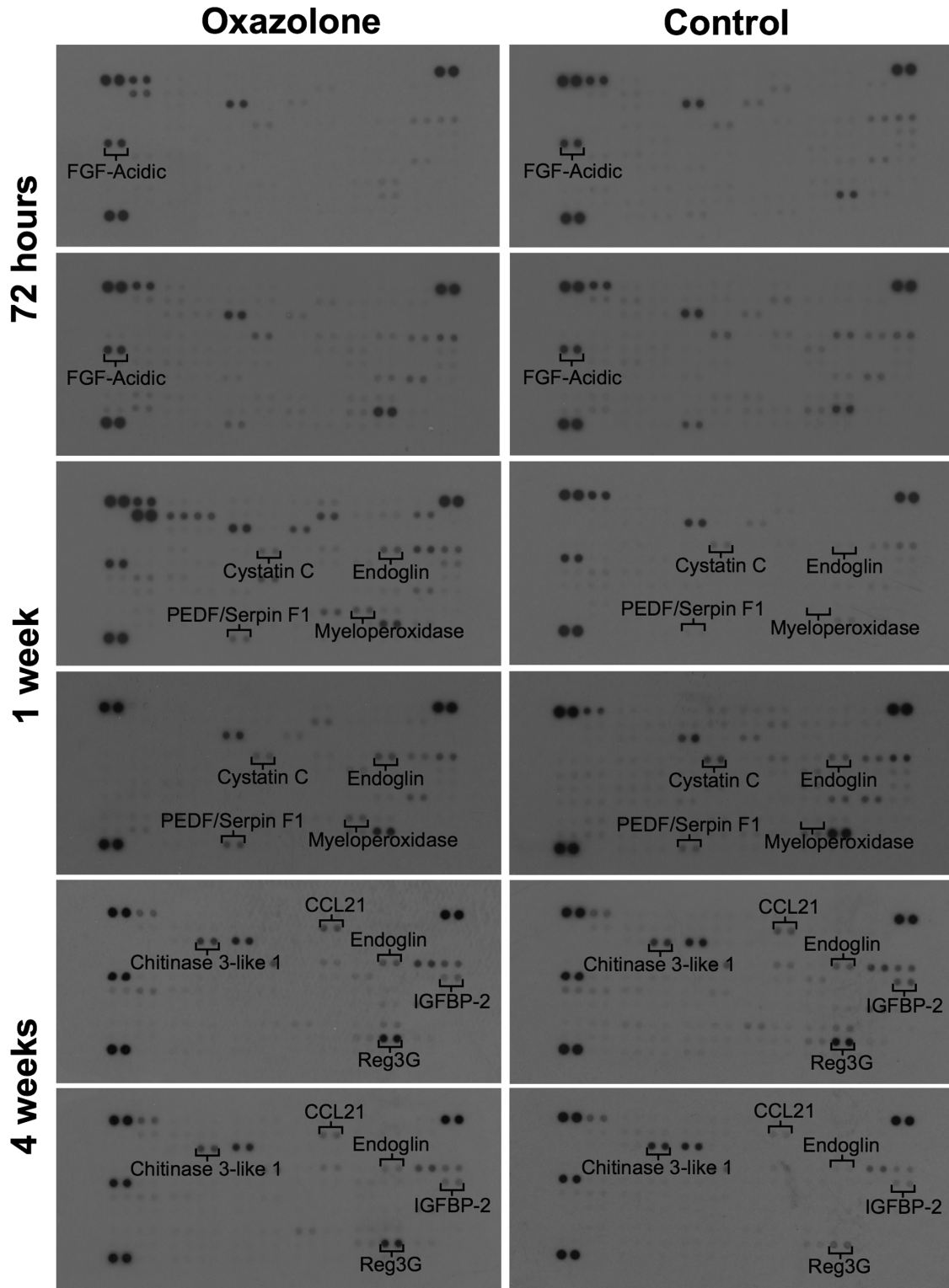


**Figure 5.** Cytokine analysis in oxazolone injected murine orbits. Dot blots represent levels of specific proteins, in technical duplicate, found in orbital tissue from two oxazolone- and pbs-injected orbits collected at 72 hours, one week, and four weeks. Acidic FGF, PEDF, cystatin C, myeloperoxidase, endoglin, chitinase 3-like 1, Reg3 $\gamma$ , CCL21, and IGFBP-2 were found to be differentially expressed compared to the pbs-injected orbit tissue.

**Table.** Fold Change of Differentially Abundant Proteins

Time Point	Mouse	Protein	Fold Change (Oxazolone/Control)
72 Hours	Mouse 1	Acidic FGF	1.75
	Mouse 2	Acidic FGF	1.01
1 Week	Mouse 3	PEDF	7.38
		Cystatin C	0.69
		Myeloperoxidase	8.79
	Mouse 4	Endoglin	8.14
		PEDF	1.55
		Cystatin C	0.56
		Myeloperoxidase	4.32
4 Weeks	Mouse 5	Endoglin	1.31
		Chitinase 3-like 1	0.88
		Reg3 $\gamma$	1.14
		CCL21	1.29
		IGFBP-2	0.70
	Mouse 6	Endoglin	1.20
		Chitinase 3-like 1	0.63
		Reg3 $\gamma$	2.22
		CCL21	1.68
		IGFBP-2	0.78

hypersensitivity reactions. As such, we have shown through immunofluorescence that there are striking similarities in the composition of inflammatory cell subsets in this mouse model compared with human orbit samples in acute TED.

Additionally, previous studies involving the cornea and orbit have shown that inflammatory states can affect proliferation of lymphatic vessels. Maruyama and colleagues<sup>21</sup> demonstrated that in the cornea, which is normally devoid of vascular structures, there is formation of new lymphatic channels when inflammation is induced. Furthermore, in our previous studies, we have demonstrated LYVE-1-positive lymphatic vessels in orbital tissue of patients with acute TED that are absent in chronic TED and in normal controls.<sup>15</sup> Our mouse model mirrors this transience of lymphatic vessels shortly after injection of oxazolone that regressed by four weeks. There is also active angiogenesis in acute TED that we have similarly demonstrated via endomucin staining in our murine model.

At 72 hours, our analyses showed a significant increase in acidic FGF, a growth factor critical for angiogenesis,<sup>23</sup> the wound healing process,<sup>24</sup> and fibrosis.<sup>25–26</sup> At the one-week time point, we identified a significant increase in PEDF, an inhibitor of neovascularization and endothelial cell proliferation and migration.<sup>27</sup> These findings suggest that the angiogenic

phase of the disease occurs early within the course of the model, and that antiangiogenic factors increase as the disease enters a more chronic phase of the model.

At the one-week time point, we found a decrease in cystatin C, a cysteine protease inhibitor commonly used as a measure of glomerular filtration rate. This protein has also been associated with immune responses to various antigens resulting in inflammatory responses.<sup>28</sup> Serum levels of cystatin C have been considered a systemic inflammatory marker for a variety of diseases including acute kidney injury,<sup>29</sup> chronic obstructive pulmonary disease,<sup>30</sup> and metabolic syndrome.<sup>31</sup> This suggests cystatin C as a potential systemic biomarker for orbital inflammation. Furthermore, with concomitant infiltration of neutrophils, we discovered as expected increased expression of myeloperoxidase<sup>32</sup> at the 1-week time point, which is an enzyme mediator of tissue damage and inflammation found in neutrophils.

At the one- and four-week time points, we identified a significant increase in endoglin, a transmembrane glycoprotein found in vascular endothelial cells whose expression is up-regulated during angiogenesis and inflammation.<sup>33</sup> This protein plays a key role in the migration of leukocytes across the vascular endothelium. Increased expression of endoglin suggests its role

in the transmigration of leukocytes in our oxazolone-induced model.

At four weeks we discovered significantly decreased expression of CHI3L1, also known as YKL-40, a well-characterized marker of inflammation.<sup>34,35</sup> YKL-40 has been considered as a serum biomarker for myriad inflammatory diseases including psoriasis,<sup>36</sup> neurodegenerative disease,<sup>37</sup> asthma,<sup>38</sup> and cancer.<sup>39,40</sup> These findings suggest CHI3L1, or YKL-40 as a potential biomarker in orbital inflammation.

Concurrently, we discovered increased expression of Reg3 $\gamma$ , a potential inhibitor of inflammatory cytokine expression.<sup>41</sup> However, at four weeks, we also observed an increase in CCL21, a chemokine expressed in dendritic<sup>42</sup> and T-cell<sup>43</sup> cell trafficking during inflammation. These findings suggest the presence of both anti-inflammatory and proinflammatory molecules at the four-week stage of our model, signifying mechanisms to regulate the acute inflammation and potentially perpetuate the late stage inflammatory state of our model.

Because of limitations of sample size, patchy involvement of the tissue, and differential stages of the disease in patients, in vivo studies of cytokine expression in patients have been variable.<sup>44</sup> Nonetheless, it has been suggested by others<sup>45,46</sup> that the acute stage of TED is regulated by Th1-like cytokines (IFN- $\gamma$ , IL-2, and TNF- $\alpha$ ), whereas the chronic stage of TED is believed to be regulated by Th2-like cytokines (IL-4, IL-5, and IL-10). Similarly, as discussed above, we observed differential cytokine expression between the acute and late stage of our model, as well as the importance of T-cell trafficking as suggest by expression of CCL21. However, although our protein assay did test for IFN- $\gamma$ , IL-2, TNF- $\alpha$ , IL-4, IL-5, and IL-10, we did not find significant differential expression of these cytokines between oxazolone-injected and control eyes as determined by our assay. We believe this difference between our model and previous human studies may be due to the decreased sensitivity of our assay (which assayed protein expression of 111 different cytokines) compared to quantitative RT-PCR (which evaluated mRNA expression of specific cytokines).<sup>44</sup>

We also found a decrease in IGFBP-2 at the four-week time point, which is involved in the regulation of insulin growth factor (IGF) signaling. The vast majority of serum IGFs are bound to IGFBP proteins. In addition to its ability to bind IGF-1 and IGF-2, IGFBP-2 can independently affect cell adhesion of endothelial progenitor cells<sup>47</sup> and has a nuclear localization signal allowing for IGF-independent transactivation activity.<sup>48</sup> IGF-1 and IGF-1R have an established impact on the mammalian immune system; specifically, they have been implicated in TED<sup>49</sup> and

medications are currently being developed and used to target IGF-1R.<sup>50,51</sup>

This study has achieved the aim of devising an animal model of immune-mediated, localized inflammation of the orbit that can consistently and reproducibly demonstrate the clinical, radiographic and histopathologic phenotype with minimal traumatic injury to ocular or adnexal structures. Although it is not known whether this model mimics the exact pathophysiology of many orbital inflammatory syndromes, including TED, it does create a comparable milieu of inflammatory cells, blood vessels, lymphatic vessels, and cytokine markers that can serve as a platform to study new therapeutic modalities to treat patients suffering from orbital inflammatory conditions.

## Acknowledgments

Supported by the National Institutes of Health grants R01-DK104641 (DRB), K12-EY16335 (LAK), R21-EY027061 (LAK), and Center Core Grant P30-EY003790. Additional support was provided by the American Thyroid Association (Falls Church, VA) (LAK) and the Massachusetts Lions Eye Research Foundation (Belmont, MA) (LAK).

Disclosure: **D. Amarnani**, None; **A.V. Sanchez**, None; **L.L. Wong**, None; **B.V. Duffy**, None; **L. Ramos**, None; **S.K. Freitag**, None; **D.R. Bielenberg**, None; **L.A. Kim**, None; **N.G. Lee**, None

\* DA and AVS contributed equally to this article.

‡ LAK and NGL contributed equally to this article.

## References

1. Garrity JA, Bahn RS. Pathogenesis of graves ophthalmopathy: implications for prediction, prevention, and treatment. *Am J Ophthalmol.* 2006;142:147–153.
2. Weber AL, Romo LV, Sabates NR. Pseudotumor of the orbit. Clinical, pathologic, and radiologic evaluation. *Radiol Clin North Am.* 1999;37:151–168, xi.
3. Wiesweg B, Johnson KT, Eckstein AK, Berchner-Pfannschmidt U. Current insights into animal models of Graves' disease and orbitopathy. *Horm Metab Res.* 2013;45:549–555.
4. Dagdelen S, Kong YC, Banga JP. Toward better models of hyperthyroid Graves' disease. *Endocrinol Metab Clin North Am.* 2009;38:343–354, viii.

5. Zhao SX, Tsui S, Cheung A, Douglas RS, Smith TJ, Banga JP. Orbital fibrosis in a mouse model of Graves' disease induced by genetic immunization of thyrotropin receptor cDNA. *J Endocrinol.* 2011;210:369–377.
6. Moshkelgosha S, So PW, Deasy N, Diaz-Cano S, Banga JP. Cutting edge: retrobulbar inflammation, adipogenesis, and acute orbital congestion in a preclinical female mouse model of Graves' orbitopathy induced by thyrotropin receptor plasmid-in vivo electroporation. *Endocrinology.* 2013;154:3008–3015.
7. Fries PD, Fohrman DS, Char DH. Phorbol ester-induced orbital myositis. *Arch Ophthalmol.* 1987;105:1273–1276.
8. Asherson GL, Ptak W. Contact and delayed hypersensitivity in the mouse. I. Active sensitization and passive transfer. *Immunology.* 1968;15:405–416.
9. Jin H, He R, Oyoshi M, Geha RS. Animal models of atopic dermatitis. *J Invest Dermatol.* 2009;129:31–40.
10. Matsumoto K, Mizukoshi K, Oyobikawa M, Ohshima H, Tagami H. Establishment of an atopic dermatitis-like skin model in a hairless mouse by repeated elicitation of contact hypersensitivity that enables to conduct functional analyses of the stratum corneum with various non-invasive biophysical instruments. *Skin Res Technol.* 2004;10:122–129.
11. Man MQ, Hatano Y, Lee SH, et al. Characterization of a hapten-induced, murine model with multiple features of atopic dermatitis: structural, immunologic, and biochemical changes following single versus multiple oxazolone challenges. *J Invest Dermatol.* 2008;128:79–86.
12. Heller F, Fuss IJ, Nieuwenhuis EE, Blumberg RS, Strober W. Oxazolone colitis, a Th2 colitis model resembling ulcerative colitis, is mediated by IL-13-producing NK-T cells. *Immunity.* 2002;17:629–638.
13. Webb EF, Tzimas MN, Newsholme SJ, Griswold DE. Intralesional cytokines in chronic oxazolone-induced contact sensitivity suggest roles for tumor necrosis factor alpha and interleukin-4. *J Invest Dermatol.* 1998;111:86–92.
14. Enk AH, Katz SI. Contact sensitivity as a model for T-cell activation in skin. *J Invest Dermatol.* 1995;105:80S–83S.
15. Wong LL, Lee NG, Amarnani D, et al. Orbital angiogenesis and lymphangiogenesis in thyroid eye disease: an analysis of vascular growth factors with clinical correlation. *Ophthalmology.* 2016;123:2028–2036.
16. Primo V, Graham M, Bigger-Allen AA, et al. Blood biomarkers in a mouse model of CADASIL. *Brain Res.* 2016;1644:118–126.
17. Many MC, Costagliola S, Detrait M, Denef F, Vassart G, Ludgate MC. Development of an animal model of autoimmune thyroid eye disease. *J Immunol.* 1999;162:4966–4974.
18. Costagliola S, Many MC, Stalmans-Falys M, Vassart G, Ludgate M. Transfer of thyroiditis, with syngeneic spleen cells sensitized with the human thyrotropin receptor, to naive BALB/c and NOD mice. *Endocrinology.* 1996;137:4637–4643.
19. Baker G, Mazziotti G, von Ruhland C, Ludgate M. Reevaluating thyrotropin receptor-induced mouse models of graves' disease and ophthalmopathy. *Endocrinology.* 2005;146:835–844.
20. Katsanos A, Asproudis I, Katsanos KH, Dastiridou AI, Aspiotis M, Tsianos EV. Orbital and optic nerve complications of inflammatory bowel disease. *J Crohns Colitis.* 2013;7:683–693.
21. Maruyama K, Ii M, Cursiefen C, et al. Inflammation-induced lymphangiogenesis in the cornea arises from CD11b-positive macrophages. *J Clin Invest.* 2005;115:2363–2372.
22. Streilein JW, Bradley D, Sano Y, Sonoda Y. Immunosuppressive properties of tissues obtained from eyes with experimentally manipulated corneas. *Invest Ophthalmol Vis Sci.* 1996;37:413–424.
23. Friesel RE, Maciag T. Molecular mechanisms of angiogenesis: fibroblast growth factor signal transduction. *FASEB J.* 1995;9:919–925.
24. Steed DL. The role of growth factors in wound healing. *Surg Clin North Am.* 1997;77:575–586.
25. Yu C, Wang F, Jin C, et al. Role of fibroblast growth factor type 1 and 2 in carbon tetrachloride-induced hepatic injury and fibrogenesis. *Am J Pathol.* 2003;163:1653–1662.
26. Barrios R, Pardo A, Ramos C, Montano M, Ramirez R, Selman M. Upregulation of acidic fibroblast growth factor during development of experimental lung fibrosis. *Am J Physiol.* 1997;273:L451–458.
27. Duh EJ, Yang HS, Suzuma I, et al. Pigment epithelium-derived factor suppresses ischemia-induced retinal neovascularization and VEGF-induced migration and growth. *Invest Ophthalmol Vis Sci.* 2002;43:821–829.
28. Zi M, Xu Y. Involvement of cystatin C in immunity and apoptosis. *Immunol Lett.* 2018;196:80–90.
29. Schanz M, Pannes D, Dippon J, Wasser C, Alscher MD, Kimmel M. The influence of thyroid function, inflammation, and obesity on risk prediction

- of acute kidney injury by cystatin C in the emergency department. *Kidney Blood Press Res.* 2016;41:604–613.
30. Zhang M, Li Y, Yang X, et al. Serum cystatin C as an inflammatory marker in exacerbated and convalescent COPD patients. *Inflammation.* 2016;39:625–631.
  31. Liu P, Sui S, Xu D, Xing X, Liu C. Clinical analysis of the relationship between cystatin C and metabolic syndrome in the elderly. *Rev Port Cardiol.* 2014;33:411–416.
  32. van der Veen BS, de Winther MP, Heeringa P. Myeloperoxidase: molecular mechanisms of action and their relevance to human health and disease. *Antioxid Redox Signal.* 2009;11:2899–2937.
  33. Rossi E, Sanz-Rodriguez F, Eleno N, et al. Endothelial endoglin is involved in inflammation: role in leukocyte adhesion and transmigration. *Blood.* 2013;121:403–415.
  34. Salomon J, Matusiak L, Nowicka-Suszko D, Szepietowski JC. Chitinase-3-like protein 1 (YKL-40) is a new biomarker of inflammation in psoriasis. *Mediators Inflamm.* 2017;2017:9538451.
  35. Salomon J, Matusiak L, Nowicka-Suszko D, Szepietowski JC. Chitinase-3-like protein 1 (YKL-40) reflects the severity of symptoms in atopic dermatitis. *J Immunol Res.* 2017;2017:5746031.
  36. Baran A, Mysliwiec H, Szterling-Jaworowska M, Kiluk P, Swiderska M, Flisiak I. Serum YKL-40 as a potential biomarker of inflammation in psoriasis. *J Dermatolog Treat.* 2018;29:19–23.
  37. Molinuevo JL, Ayton S, Batrla R, et al. Current state of Alzheimer's fluid biomarkers. *Acta Neuropathol.* 2018;136:821–853.
  38. Gomez JL, Yan X, Holm CT, et al. Characterisation of asthma subgroups associated with circulating YKL-40 levels. *Eur Respir J.* 2017;50(4):1700800.
  39. Wan G, Xiang L, Sun X, et al. Elevated YKL-40 expression is associated with a poor prognosis in breast cancer patients. *Oncotarget.* 2017;8:5382–5391.
  40. Chen HT, Zheng JM, Zhang YZ, et al. Overexpression of YKL-40 predicts poor prognosis in patients undergoing curative resection of pancreatic cancer. *Pancreas.* 2017;46:323–334.
  41. Ito T, Hirose K, Saku A, et al. IL-22 induces Reg3gamma and inhibits allergic inflammation in house dust mite-induced asthma models. *J Exp Med.* 2017;214:3037–3050.
  42. Johnson LA, Jackson DG. Inflammation-induced secretion of CCL21 in lymphatic endothelium is a key regulator of integrin-mediated dendritic cell transmigration. *Int Immunol.* 2010;22:839–849.
  43. Alt C, Laschinger M, Engelhardt B. Functional expression of the lymphoid chemokines CCL19 (ELC) and CCL 21 (SLC) at the blood-brain barrier suggests their involvement in G-protein-dependent lymphocyte recruitment into the central nervous system during experimental autoimmune encephalomyelitis. *Eur J Immunol.* 2002;32:2133–2144.
  44. Hiromatsu Y, Yang D, Bednarczuk T, Miyake I, Nonaka K, Inoue Y. Cytokine profiles in eye muscle tissue and orbital fat tissue from patients with thyroid-associated ophthalmopathy. *J Clin Endocrinol Metab.* 2000;85:1194–1199.
  45. Natt N, Bahn RS. Cytokines in the evolution of Graves' ophthalmopathy. *Autoimmunity.* 1997;26:129–136.
  46. Gianoukakis AG, Khadavi N, Smith TJ. Cytokines, Graves' disease, and thyroid-associated ophthalmopathy. *Thyroid.* 2008;18:953–958.
  47. Feng N, Zhang Z, Wang Z, et al. Insulin-like growth factor binding protein-2 promotes adhesion of endothelial progenitor cells to endothelial cells via integrin alpha5beta1. *J Mol Neurosci.* 2015;57:426–434.
  48. Zhao Y, Yin P, Bach LA, Duan C. Several acidic amino acids in the N-domain of insulin-like growth factor-binding protein-5 are important for its transactivation activity. *J Biol Chem.* 2006;281:14184–14191.
  49. Hoa N, Tsui S, Afifiyan NF, et al. Nuclear targeting of IGF-1 receptor in orbital fibroblasts from Graves' disease: apparent role of ADAM17. *PLoS One.* 2012;7:e34173.
  50. Smith TJ, Hegedus L, Douglas RS. Role of insulin-like growth factor-1 (IGF-1) pathway in the pathogenesis of Graves' orbitopathy. *Best Pract Res Clin Endocrinol Metab.* 2012;26:291–302.
  51. Smith TJ, Kahaly GJ, Ezra DG, et al. Teprotumumab for Thyroid-Associated Ophthalmopathy. *N Engl J Med.* 2017;376:1748–1761.